# Constrained Bayesian Accelerated Design of Acoustic Polyurethane Coatings with Metamaterial Features Under Hydrostatic Pressure

Pengyuan Ding[1], Dominic Robe[1], Michael Kirley[2], Elnaz Hajizadeh[1*]

[1*]Soft Matter Informatics Research Group, Department of Mechanical Engineering, Faculty of Engineering and Information Technology, The University of Melbourne, Parkville, Australia.

[2]School of Computing and Information Systems, The University of Melbourne, Parkville, Australia.

*Corresponding author(s). E-mail(s): ellie.hajizadeh@unimelb.edu.au;
Contributing authors: pding@student.unimelb.edu.au; nick.robe@unimelb.edu.au; mkirley@unimelb.edu.au;

**Abstract**

Here we propose a novel, fully automated framework for accelerated design of underwater acoustic coatings, targeting the reduction of acoustic signature of naval platforms under operational conditions, by coupling Bayesian Optimization (BO) with a 2-step Finite Element Model (FEM). The developed FEMs evaluate the acoustic performance of polyurethane (PU) coatings with embedded metamaterial features under the influence of varying depth of operation i.e., hydrostatic pressure-dependent acoustic attenuation. The frequency-dependent viscoelasticity, which has often been ignored in previous studies, is also considered in the FEMs to obtain a realistic evaluation of the absorption behavior of these coatings over a wide range of operational frequencies. The main contribution of the proposed optimization framework is its efficient utilization of the expensive FEM simulations through BO. The desired broadband and low-frequency attenuation is achieved under the varying operating depth by an optimal design of the void layers. Moreover, this framework enables the targeted design of underwater acoustic coatings by effective exploration of the 10-dimensional, vast and computationally expensive design space, leading to a significant reduction in the number of simulations required to run compared to conventional exhaustive search strategies.

**Keywords:** Underwater Acoustic Coatings, Bayesian Optimization, Hydrostatic Pressure, Viscoelastic, Acoustic Metamaterials

## 1 Introduction

Underwater radiated noise management is crucial for two main reasons, namely 1) mitigating the negative impacts of anthropogenic noise and 2) reducing the acoustic signature and hence increasing the survivability and operational effectiveness of naval platforms. Therefore, acoustic coating materials have been continuously developed and installed on naval platforms to attenuate sound

against active and passive sonar systems. Modern sonar systems are particularly effective in the low-frequency range, where achieving effective sound absorption has traditionally been difficult [1]. Elastomeric materials, known for their tunable and favorable viscoelastic properties, are widely used as base materials for acoustic coatings [2]. In theory, low-frequency sound absorption improves with increased coating thickness, as thicker layers offer a longer path for sound wave dissipation. However, practical applications impose strict constraints on the thickness of coatings due to limitations in weight, space, and structural stability, making it impossible to achieve optimal low-frequency absorption through increased thickness alone.

To address this limitation, metamaterials, i.e., resonant inclusions arranged in repeating patterns in elastomeric matrix materials have emerged as a promising solution [3]. These inclusions, strategically embedded within the matrix material, collectively generate a low-frequency sub-wavelength absorption effect that enhances sound attenuation across a wider frequency range than a homogeneous material could achieve alone, thus compensates for the constraints on thickness.

Viscoelastic materials and resonant inclusions have been extensively studied, but most of them were modeled without considering the influence of the hydrostatic pressure arising from operations at depth. For example, in the absence of pressure effects, Sharma et al. [4] found that in a voided rubber coating with a steel backing plate, sound absorption is strongly dependent on Fabry-Pérot mass-spring resonance; they also found that the steel backing significantly affects acoustic performance. In another work, they developed analytical models to predict the monopole resonance frequency of an array of cylindrical voids embedded in soft elastic medium [5] and sound transmission, reflection and absorption of such materials [6]. In addition, geometric parameters have been found to have a significant impact on the performance of acoustic coatings [7].

However, hydrostatic pressure has also been shown to have a considerable impact on the acoustic behavior of these materials [8]. A limited number of studies have addressed the effect of hydrostatic pressure, typical of the operational depths of naval platforms, in their study of the acoustic performance of these coatings. Fu et al. [9] studied the impact of hydrostatic pressure on a PDMS matrix embedded with periodic cylinders using a numerical model. Fang et al. [10] investigated low-frequency acoustic performance of such metamaterial under hydrostatic pressure using an analytical model. Both studies simplified their models of materials by ignoring the frequency-dependency of the viscoelastic moduli and only considered unrealistic constant complex number for the moduli.

The acoustic properties of viscoelastic materials[11–13] are inherently frequency-dependent, and we have shown in our previous study [14] that the frequency-dependency has significant impact on the acoustic behavior of these coatings. However, deformation of the metamaterial induced by hydrostatic pressure is time-dependent. Existing methods, such as finite element modeling (FEM), typically evaluate the two problems separately and have no direct way to integrate them. This gap highlights the need for a more integrated modeling framework.

To overcome these challenges, here, we develop a two-stage FEM simulation that systematically incorporates the hydrostatic pressure effects into the acoustic analysis, which enables a comprehensive evaluation of the sound-absorbing performance of metamaterials under realistic underwater conditions.

Several optimization approaches for the structural design of metamaterials have been explored in the literature [9, 10, 14, 15]. Fu et al. [9] used Nelder–Mead algorithm to optimize the size and location of a single layer of cylindrical voids within the PDMS matrix. Fang et al. [10] leveraged the analytical model to develop a genetic algorithm for optimization. In our previous study [14], we also developed a genetic algorithm integrated with a deep neural network for simulating the acoustic performance.

Although these methods have been effective in previous research, they face significant limitations when dealing with frequency-dependent viscoelasticity under hydrostatic pressure. The high computational expense of simulating with frequency-dependent moduli makes evolutionary algorithms, such as genetic algorithms, impractical due to their excessive runtime. Additionally, generating sufficient data for training an accurate neural network that accommodates the infeasible solution

space becomes a considerable challenge [16]. To address these difficulties, we employ a Bayesian Optimization (BO) framework, which is proven to offer a superior search strategy [17], where objective function evaluation is expensive, and infeasible regions are unknown [18, 19]. We showed in our previous research [17, 20] that Bayesian framework reduces the number of simulations required to optimize polymer model parameters by one order of magnitude compared to a DNN framework.

To the best of our knowledge, there has been no previous study on optimization of acoustic coatings based on polyurethane[21] metamaterials with consideration of both the effect of frequency-dependent viscoelastic properties of the matrix and operational depth i.e., hydrostatic pressure, simultaneously. The integrated framework presented in this study, therefore, bridges a critical gap in acoustic materials research by integrating the structural effects of hydrostatic pressure with the frequency-dependent acoustic properties of viscoelastic materials into a unified optimization framework. This approach not only provides a more accurate understanding of the material's performance under realistic operational conditions but also brings an acceleration to the realm of metamaterial design. By maintaining robust sound absorption across low frequencies in high pressure environments, the proposed framework offers a transformative solution for deep-sea acoustic wave attenuation applications.

The manuscript is organized as following, Section 2 describes the components of the developed optimization framework, including the FEM description (Sect. 2.1) and the Bayesian Optimization scheme (Sect. 2.2). Section 3 discusses the findings of this study in multiple subsections. Section 3.1 focuses on the effect of hydrostatic pressure, on the geometric layout and the acoustic performance of optimal design. Sect 3.2 compares and discusses optimized designs based on three commercially available polyurethane matrices (PU80 3.2.1, PU65 3.2.2 and PU95 3.2.3) with different stiffness levels. Finally, Section 4 summarizes the conclusions, emphasizing the potential of this BO framework in inverse design of acoustic coatings and other materials systems.

# 2 Methodology

## 2.1 FEM model

We model a metamaterial system composed of polyurethane elastomer as a matrix material modified with two layers of periodically distributed cylindrical voids containing air, attached to a steel backing that simulates the hull of a naval platform. The system is modeled in 2-dimensions (D) due to the unpractical computational costs associated with a three-dimensional FEM simulation across a large computational domain. A prior study [22] has validated the effectiveness of a 2D approach. Figure1a shows the cross-section of a unit cell of the 2D physical model of the coating system. The unit cell contains two layers of two cylindrical voids, with varied spacing between voids. The voids within a layer have equal radius.

The geometric design space has 10 degrees of freedom in total, including $D_1$, $D_2$, $B_1$, $B_2$, $B_3$, $B_4$, $r_1$, $r_2$, $t$ and $h$ as shown in Figure1b, representing the spacing between voids, radii of voids, thickness and height of the polyurethane matrix, respectively. The ranges of their values are listed in Table1. The goal is to find the best performing metamaterial by optimizing the geometrical parameters in three candidate base polyurethane materials with different hardness under the operational conditions, of which the environmental variables and their ranges are listed in Table2.

| **Design variable** | **Lower bound (mm)** | **Upper bound (mm)** |
|---|---|---|
| $r_1, r_2$ | 2 | 15 |
| $D_1, D_2$ | 10 | 80 |
| $B_1, B_2, B_3, B_4$ | 10 | 80 |
| $h$ | 30 | 80 |
| $t$ | 30 | 80 |

**Table 1**: Design variables and their bounds

| **Variables** | **Range/Value** |
|---|---|
| Frequencies | 100 - 10000 Hz |
| Depths | 0 - 600 m |

**Table 2**: Studied operational conditions.

We have developed a fully coupled acoustic-structure FEM model in the COMSOL Multiphysics Software Package version 6.2, to study the underwater sound absorption performances of metamaterials under various hydrostatic pressures, ranging from 1 to 6 MPa. For individual simulations, static pressure loads and sound propagation are typically handled as separate models, requiring data transfer between them. In this coupled model, we integrate both steps. First, structural deformation under static pressure is computed in the stationary "Solid Mechanics" module. Then, the deformed geometry is imported automatically to the second step, which is coupled with the "Pressure Acoustics, Frequency Domain" module, in which the sound absorption coefficient is derived under plane wave incidence.

We developed a Python script using the MPh package [23], JPype module [24] and COMSOL's built-in Java API, to implement this approach, which is later integrated into the BO framework. This implementation enables automatic construction and importation of the deformed geometries for evaluation of acoustic response, bypassing the need for manual secondary modeling, which is vital for the full automation of the whole optimization process. In the FEM model shown in Figure2b, which assumes a one-dimensional incident plane wave from water, the PU matrix and steel plate are modeled as solid domains, while water and air are treated as acoustic fluid domains. Boundary conditions include, hydrostatic pressure, acoustic-structure coupling to simulate interactions between solid and the fluid media, continuity conditions at interfaces, and free boundary conditions at void-PU boundaries. Periodic boundary conditions why? are applied on the top and bottom boundaries to simulate the structural periodicity in the y-direction, and perfectly matched layers (PMLs) to terminate outgoing waves to prevent reflection. Reflection is measured at the water-PU interface, and transmission pressure was measured at the steel-air interface.

To develop accurate models of the viscoelastic materials, we considered temperature and frequency-dependent complex Young's modulus. The master curves were generated based on experimental data measured using dynamic mechanical analysis (DMA) and adopted from our previous work [14].

The experimental setup closely follows our previous study[14]. The polymer domain and steel are modeled as viscoelastic solid and elastic solid materials, respectively. The densities of PU and steel were taken as 1026 $kgm^{-3}$ and 7850 $kgm^{-3}$, respectively at temperature T = 15°$C$ and atmosphere pressure P = 101.325 $kPa$. The thickness of the steel backing was considered 30 mm. For air and water, the inbuilt material properties available in the COMSOL materials library are used. The developed FEM models have been validated against data from literature [25, 26]. The governing wave equations were solved numerically, and the absorption coefficient $\alpha$ is calculated as Equation 1:

$$\alpha = 1 - (|T|^2 + |R|^2), \tag{1}$$

where $T$ and $R$ are transmission and reflection coefficients, respectively. Next, the evaluated absorption coefficients are passed on to the optimization algorithm, illustrated in Figure 2a.

## 2.2 Bayesian Optimization

Bayesian Optimization (BO) is a powerful global optimization framework designed for evaluation of expensive black-box functions [27], where derivative information is unavailable, and function evaluations are costly [28]. Unlike traditional optimization methods [29], BO leverages probabilistic models (commonly Gaussian Processes) to estimate the objective function and guide the search towards the global optimum with minimal evaluations.

Due to the nonlinear relationship between structural parameters and the absorption coefficient under hydrostatic pressure, analytical methods are impractical for finding an optimal solution. Additionally, with the high dimensionality in a vast design space, each FEM simulation becomes computationally expensive, requiring an efficient method to balance the exploration-exploitation trade-offs for the optimization process. Hence, given the nature of our problem, BO proves to be the appropriate optimization framework.

To achieve a low-frequency broad-band absorption, we chose the objective function of our BO as a frequency-weighted and depth-weighted

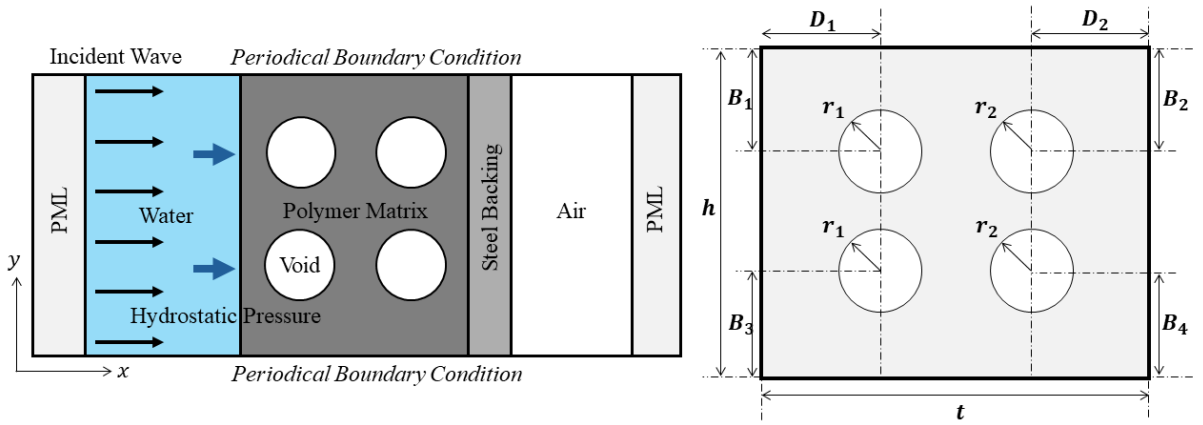


(a) (b)

**Fig. 1**: **a** 2D schematic diagram of the unit cell of model elastomer matrix composite with four cylindrical voids. **b** Schematic representation of the design space including the geometrical variables for the 2D COMSOL model.

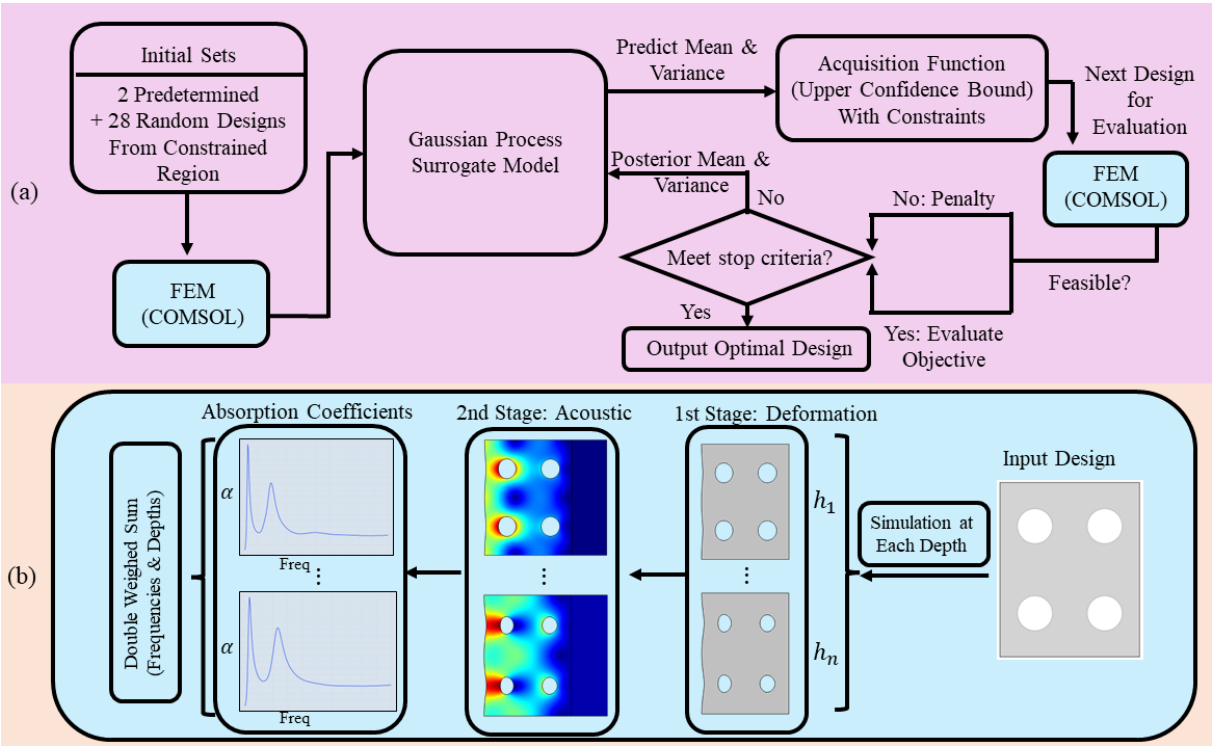


**Fig. 2**: **a** The schematic representation of the proposed Bayesian optimization framework (pink online). **b** Schematic representation of the 2-step FEM COMSOL model (blue online).

sum of the absorption coefficients, which is to be maximized, as shown in the Equation 2:

$$\max \begin{cases} p & \text{infeasible} \\ \sum_{j=1}^{M} w_j^d \left( \sum_{i=1}^{N} w_i^f \alpha_{i,j} \right) & \text{otherwise,} \end{cases} \quad (2)$$

where $\alpha_{i,j}$ represents the absorption coefficient for certain frequency at certain depth in water; $w_i^f$ represents the weight of each frequency in the summation, which is higher for the lower frequencies, to guide the algorithm to achieve a low-frequency broad-band absorption; $w_j^d$ represents the weight of each depth of operation, which in this study were set as equal except for a doubled weight for 300 m which is designated as the most common operational depth; and $p$ represents the penalty that accounts for manufacturing or practical constraints that would lead to infeasible solutions otherwise. At each iteration, objective function evaluates $\alpha_{i,j}$ by calling the FEM. The range of frequencies studied is $1 \sim 10^4 Hz$.

The BO framework iteratively refines its estimation of the objective function using a Bayesian surrogate model and an acquisition function. The surrogate model is used to approximate the objective function and to provide a probabilistic estimate of the function's values and uncertainty at unexplored points. Whereas acquisition function determines the next point to sample by balancing exploration (sampling uncertain regions) and exploitation (sampling regions likely to improve the objective). Thus it minimizes the number of expensive evaluations needed to identify the global optimum compared to traditional exhaustive or Brute force search strategies. In this study we chose Gaussian Process (GP) as the surrogate model, which is proven to be effective for low-medium dimensional problems [30], and Upper Confidence Bound (UCB) as the acquisition function, which balances between local exploitation and global exploration [31].The fully-automated integrated BO framework then is developed in Python (version 3.10.9) using the Bayesian Optimization package [32]. The size of the initial set to construct the surrogate GP was set as 30, consisting of 2 pre-determined and 28 randomly generated designs. The number of iterations was set as 100.

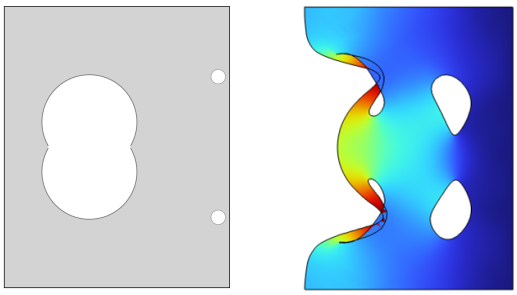

(a) Type I infeasibility (b) Type II infeasibility

**Fig. 3**: Two types of possible infeasible designs.

### 2.2.1 Infeasible solution space

In the search for the optimal topological design of the acoustic materials under hydrostatic pressure, the design space for viable configurations exhibits a non-uniform and fragmented distribution, characterized by regions of infeasible combinations of geometric parameters interspersed throughout the search domain. These infeasible configurations can be categorized into two distinct types:

**Type I: Initial Design Constraints**

This type includes invalid initial topological configurations, such as overlapping voids or voids exceeding the matrix boundary, as shown in Figure3a. These issues can be identified analytically before running the simulations.

**Mitigation Strategy:** Type I configurations were modeled as constraints within the BO framework by modifying the acquisition function, so that the optimizer avoids sampling points that are likely infeasible [19, 32]. This adjustment significantly reduces the likelihood of sampling within the invalid regions, thus improving the computational efficiency of the BO process.

**Type II: Simulation-Induced Failures**

This type arises from numerical instabilities or structural failures under hydrostatic pressure, such as void collapse, as shown in Figure3b. These issues can only be detected during or after a simulation.

**Mitigation Strategy:** For Type II configurations, a penalty was applied via assigning a very low objective value to the failed designs. This penalty mechanism encourages the algorithm to avoid these regions in subsequent iterations. It is worth mentioning that the simulation process was carefully designed to automatically restart after

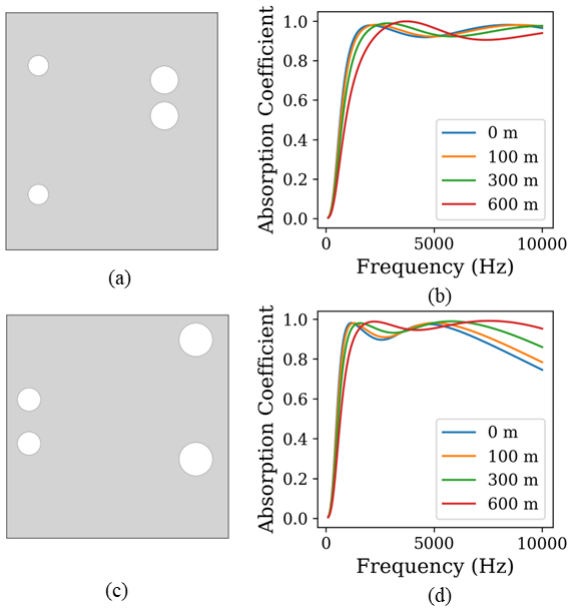


**Fig. 4**: **a** Optimized design of PU80 at atmospheric pressure. **b** Design **a**'s performance at depth 0 m, 100 m, 300 m and 600 m. **c** Optimized design of PU80 for overall performance across depths with hydrostatic pressures. **d** Design **c**'s performance at depth 0 m, 100 m, 300 m and 600 m.

encountering an error, preventing propagation of erroneous results and ensuring the stability of the optimization process.

# 3 Results and Discussion

## 3.1 Effect of hydrostatic pressure

We have investigated the impact of hydrostatic pressure on the performance of metamaterial designs under operational conditions, by evaluating the acoustic performance of the metamaterial design optimized at atmospheric pressure (shown in Figure4a) for PU80 matrix material, at different depths under hydrostatic pressure. The results are presented in Figure4b. In addition, we also obtained the design achieving the optimal acoustic performance across all operational depths (Figure4c), of which the performances are shown in Figure4d. Comparing the performances of the two designs, we can see that the former design shows noticeably worse acoustic performance at the desired lower frequencies. Also, as the depth increases, the performance gap increases even more significantly at these frequencies (0.5 vs 0.85 at 500 Hz, 600 m). This demonstrates that the design is susceptible to performance degradation under deep water. Our more comprehensive approach eliminates such risk.

We can also see that the increased hydrostatic pressure shifts the peaks of the absorption coefficient to higher frequencies, which is in agreement with the literature [33–35].

## 3.2 Optimized designs for different polyurethane matrices

Figure5a-c shows the optimized designs of acoustic coatings for three different PU matrix materials. Figure5d-f shows the deformation maps for the same coatings under hydrostatic pressure at 300 m. From the results shown in Figure5g, it is evident that the shift in the frequency of the absorption coefficient peaks toward higher frequencies with increasing hydrostatic pressure is consistent for all polyurethane cases. We can also see that, although the values of the first peak only change slightly, there are noticeable changes in the location and intensity of the second peaks. It is worth noting that the acoustic performance is not monotonically correlated to the stiffness of the material, but rather more influenced by the frequency-dependent moduli, even though the optimized void radii show a monotonic increasing trend with stiffness values (illustrated in the following subsections).

In our previous study [14], we showed that the first peak of absorption coefficients is attributed to the second layer of voids, while the second peak is attributed to the first layer. We find that this conclusion is consistent with our study taking into account the hydrostatic pressure (see Fig. 6). It also explains the magnitude of changes in peak values of absorption coefficients. The deformation caused by hydrostatic pressure is larger on the first layer of voids and relatively smaller on the second layer, which naturally produces more significant impact of pressure on the high frequency absorption peak.

The selection of an appropriate matrix material plays a critical role in the optimization of acoustic coatings, especially when void-based geometries are employed. This section presents a comparative analysis of three polyurethane (PU)

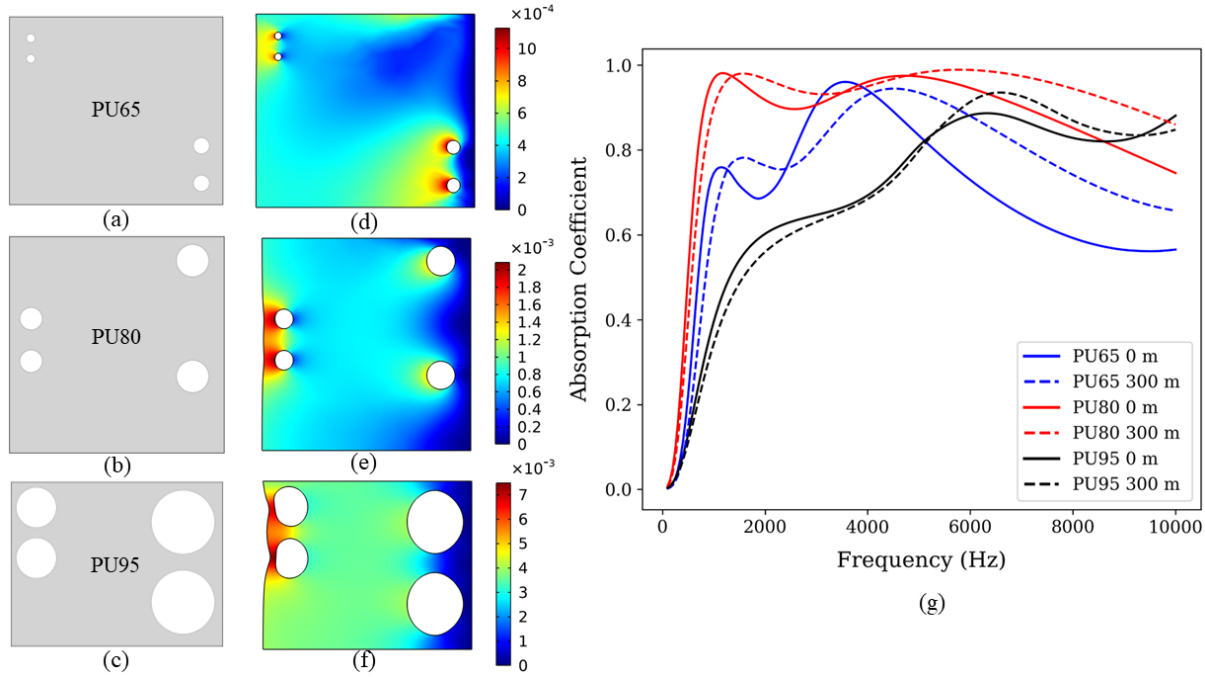


**Fig. 5**: **a-c** Optimized design for PU65, PU80, and PU95. **d-f** Deformation caused by hydrostatic pressure of the optimized designs at 300 m depth in PU65, PU80, and PU95, unit: **m**. **g** Absorption coefficients of optimized coating of PU60 (blue), PU80 (red), PU95 (black) at 0 m (solid) and 300 m (dashed).

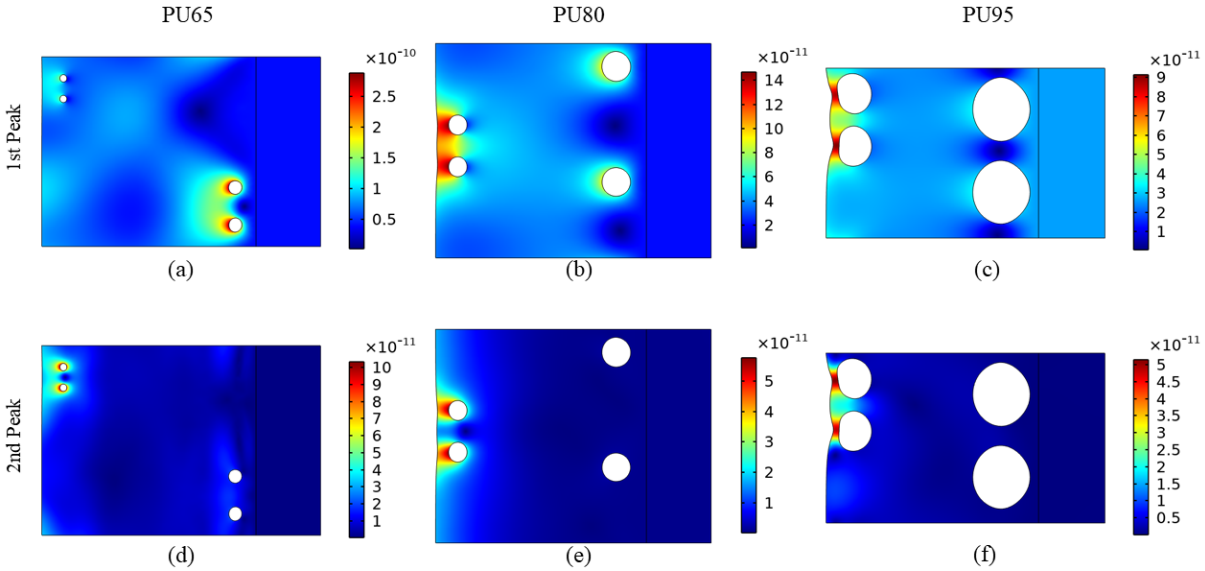


**Fig. 6**: Deformation caused by acoustic pressure at the first peak frequencies **(a-c)**, and at the second peak frequencies **(d-f)** of the optimized design at 300 m depth in PU65, PU80 and PU95, unit: **m**.

matrices, which are coded PU65, PU80, and PU95, where the numbers following 'PU' represent the stiffness of the material, and PU65 being the softest material and PU95 the hardest one. Each material was optimized using our Bayesian framework to maximize acoustic absorption performance while addressing structural integrity under varying hydrostatic pressure conditions. We obtained optimized designs for the three PU materials at depths ranging from 100 m to 600 m, and frequencies ranging from $10^2$ to $10^4$ Hz. Figure5 shows the optimized designs, the deformation under hydrostatic pressure at 300 m depth, and the acoustic performances of the three different matrix materials. This figure illustrates that as the matrix material becomes softer, the optimal radius of the voids becomes smaller to avoid collapsing under high hydrostatic pressure.

### 3.2.1 Optimized design for PU80

Figure7a illustrates the geometric configuration of the optimal design for the PU80 matrix obtained through BO. The absorption performance of this optimized coating is characterized by two prominent peaks, as shown in the same figure. These peaks occur in the frequency ranges of 1200 - 2250 Hz and 4700 - 7550 Hz, with absorption coefficients ranging from 0.9796 - 0.9878 and 0.9748 - 0.9919, respectively, with a general trend to stretch horizontally and shift to higher frequencies with increased depth. These consistently high broad-band absorption values under relevant depths of operations indicate that the optimized PU80 coating is highly effective in reducing the acoustic signature of naval platforms.

The first peak is attributed to the Fabry-Pérot acoustic resonator phenomenon, which stems from constructive interference between sound waves repeatedly reflecting back and forth within the confined space of the steel backing and the second layer of voids[14].

### 3.2.2 Optimized design for PU65

The optimization results for the PU65 matrix are presented in Figure8a-d, showing significant changes in both the geometric layout and absorption performance of these coatings compared to the PU80 design, where the voids in the softer PU65 matrix are substantially smaller, reflecting the need to prevent structural failure under high-pressure conditions. Smaller voids reduce the risk of collapse, addressing type II infeasibility and ensuring the durability of the coating.

These geometric adjustments lead to shifts in the absorption peaks, which now occur at higher frequencies compared to the PU80 matrix. Its first peaks appear between 1150 - 2350 Hz, ranging between 0.7592 - 0.8349; and second peaks appear between 3550 - 6300 Hz, ranging between 0.9404 - 0.9604. The observed shifts can be attributed to the changes in size and spatial configuration of the void layers, which alter the wave scattering. For example, smaller voids increase the effective stiffness of the coatings compared to those with larger voids, influencing the interaction between acoustic waves and the material layers.

### 3.2.3 Optimized design for PU95

The optimal geometry and performance results for the coating systems based on PU95 matrix are illustrated in Figure9a. The increased stiffness of the PU95 material allows for larger void diameters compared to PU65, without risking structural failure under hydrostatic pressure. This flexibility in void design enables the optimization framework to explore larger voids, which in theory could enhance absorption at lower frequencies.

However, the results indicate a significant reduction in absorption performance in the low-mid frequency range compared to the PU80 and PU65 matrices. The acoustic behavior also becomes more complicated: at higher depth, instead of showing a clear first peak, the absorption coefficient curve enters into a plateau-like behavior; and at all depths, rather than having a clear single second peak, PU95 shows a twin-peak phenomenon in mid-high frequency range. The first peaks/plateaus appear between 1450 - 3000 Hz, ranging between 0.6254 - 0.6730; and the twin-peaks appear between 5450 - 7300 Hz, ranging between 0.9670 - 0.9997. The decline in low-mid frequency range behavior could be attributed to the increased stiffness of the material, which reduces the material's ability to dissipate acoustic energy through void-based scattering mechanisms. At higher frequencies, PU95 retains competitive absorption performance, suggesting its potential suitability for applications where high-frequency sound is a primary concern.

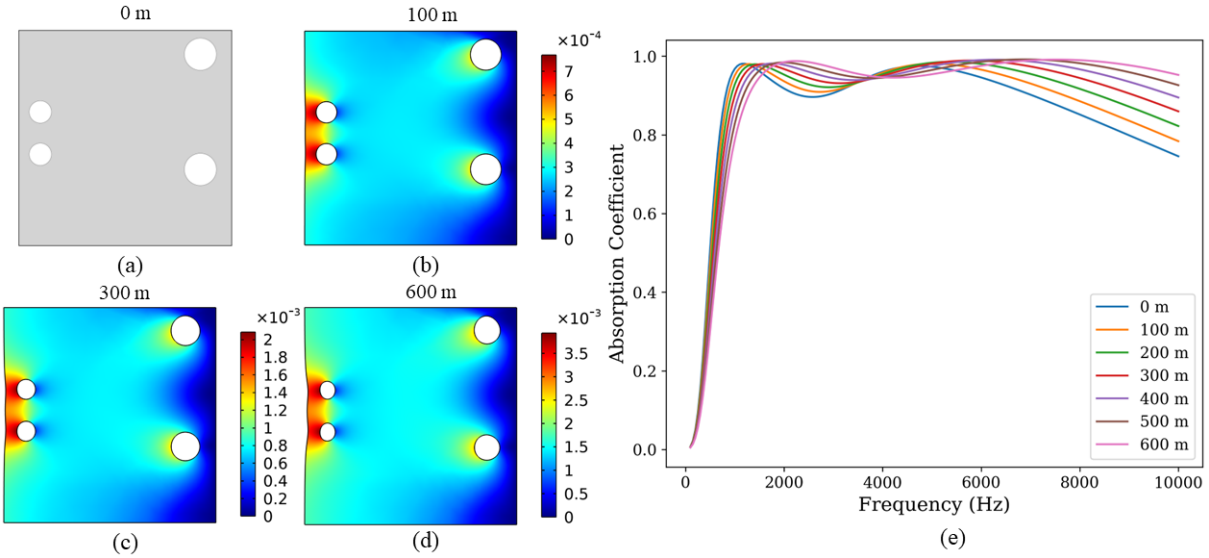


**Fig. 7**: **a** Optimized design for PU80. **b-d** Deformation maps of the optimized design in PU80 at 100 m, 300 m, 600 m, unit: **m**. **e** Absorption coefficients of optimized coating based on PU80.

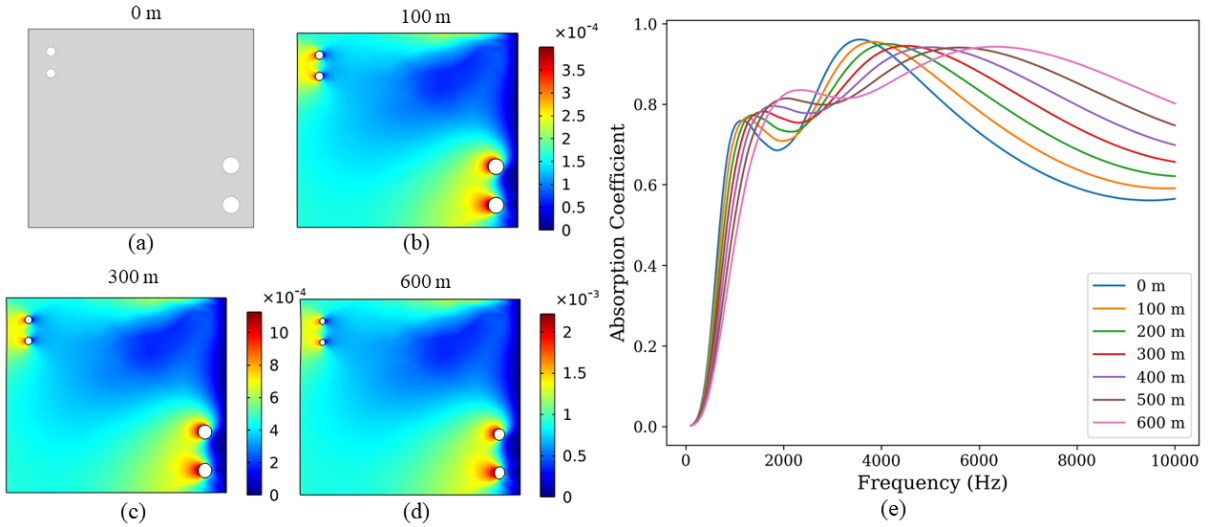


**Fig. 8**: **a** Optimized design for PU65. **b-d** Deformation maps of the optimized design in PU65 at 100 m, 300 m, 600 m, unit: **m**. **e** Absorption coefficients of optimized coating based on PU65.

These results highlight the importance of material selection in optimizing the performance of acoustic coatings, to meet desired performance requirements. Although, coatings based on PU95 demonstrate advantages such as structural stability at high depths, its reduced absorption efficiency in critical frequency ranges may limit its applicability in scenarios requiring low-frequency broad-spectrum noise attenuation.

### 3.2.4 Convergence Analysis

Figure 10a compares the convergence trends of the optimization algorithm for the three different PU matrices. It is obvious that the rates of convergence are highly dependent on the choice of matrix

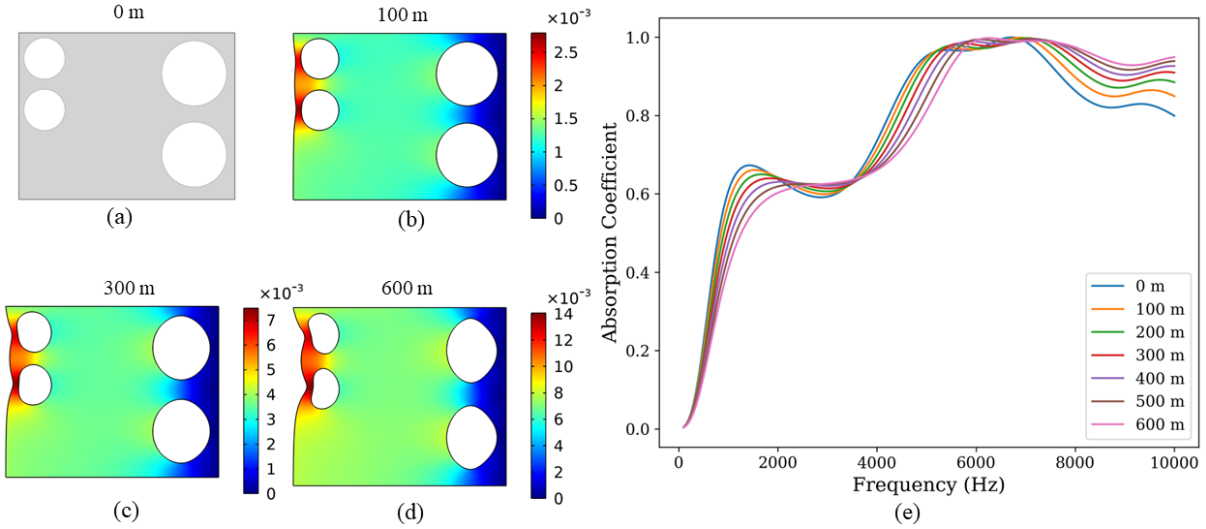


**Fig. 9**: **a** Optimized design for PU95. **b-d** Deformation maps of the optimized design in PU95 at 100 m, 300 m, 600 m, unit: **m**. **e** Absorption coefficients of optimized coating based on PU95.

materials. There are relatively large improvements at early stages of optimization in stiffer materials, which is missing in PU65. However, the clear converging trends toward the 100th iteration shown in softer materials such as PU65 and PU80 is also missing in PU95.

Figure 10b shows the optimized designs at the 15th, 50th and 100th iterations of the BO optimization for PU80, and their corresponding absorption coefficients, respectively. We can see that once the acoustic performance is close to converging, the result is robust in terms of disturbance in changes of some geometric parameters (e.g. distance between the same layer of voids, matrix height); however, may be sensitive to others (e.g. radii of the voids).

## 3.3 Design Objectives

Depending on the application, design objectives can vary. To assess the effect of different design objectives, we have designed two case studies per below.

### 3.3.1 Case A: overall optimization for a range of operational depths

The most general application requires an overall optimization of the acoustic performance for a range of operational depths rather than a single depth. Our main study, therefore, tackles this problem using a weighed average sum of the absorption coefficients per Equation 2.

### 3.3.2 Case B: optimization for a single depth

To investigate the performance of coatings and their operational effectiveness at a certain depth, we also perform optimization at each depth, separately. The optimized designs yielded distinct geometrical configurations for each target depth. Figure11 illustrates these configurations, highlighting variations in void diameter, spacing, and layout across depths.

We then compared the performances at each depth between the Case A (overall-optimization) design, obtained in Section 3.2.1, and the Case B (single-depth-optimization) design. It is noticeable in Figure11 that when hydrostatic pressure is relatively low, the gap between performances of the 2 designs are small, both in terms of the objective and the absorption coefficients at each frequency, but when hydrostatic pressure is relatively high, the difference becomes more significant. As a result, when the application is designated for a stable but high hydrostatic pressure environment, the single-depth-optimization method should be adopted.

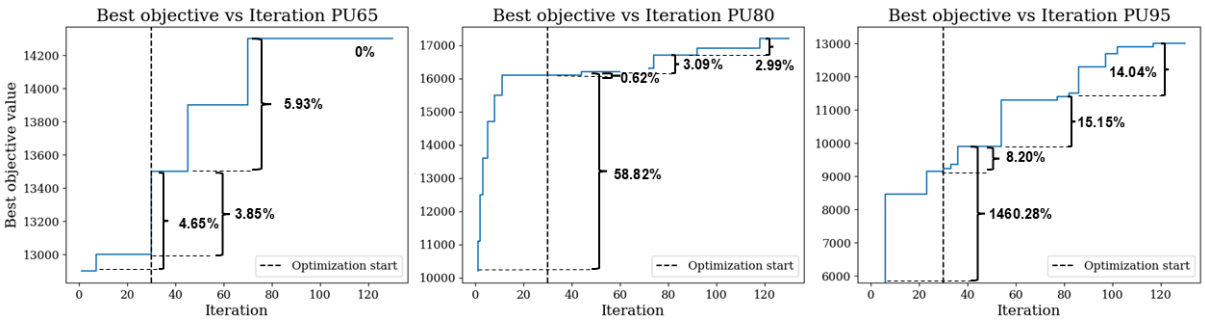


(a)

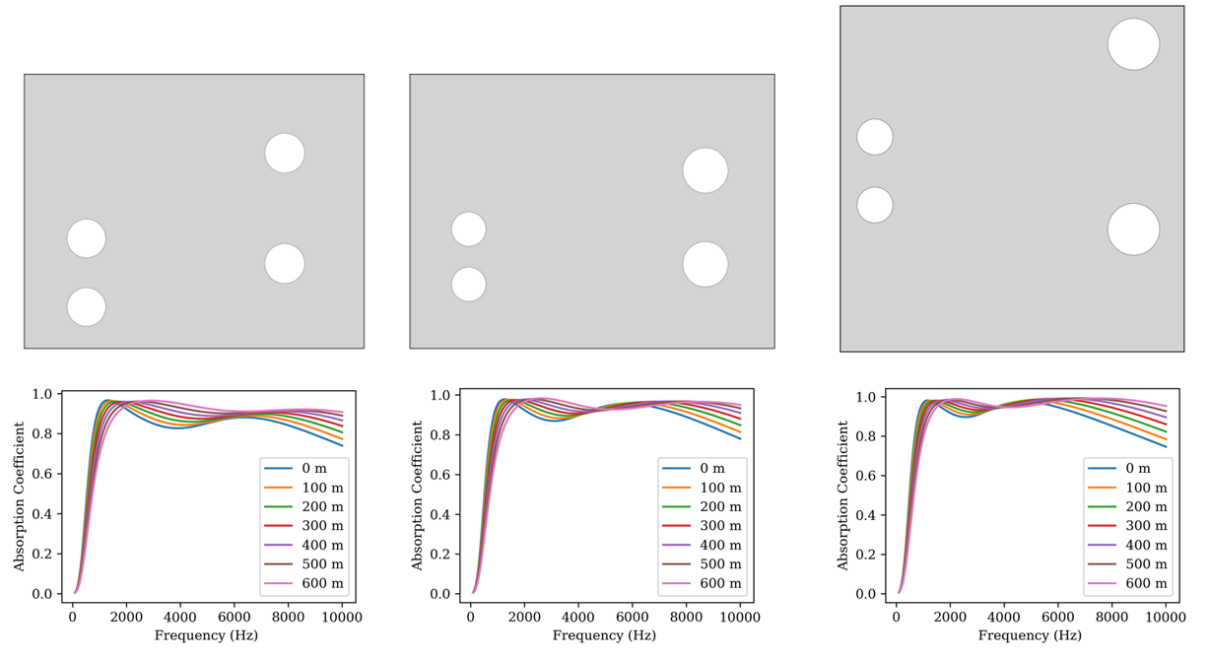


(b)

**Fig. 10**: **a** Convergence curves of (from left to right) PU65, PU80 and PU95 (In order to clearly show the percent change in objective values, different vertical scales are used here). **b** Optimized designs (top) and the corresponding absorption coefficients (bottom) at 15th, 50th and 100th iteration (from left to right) of BO optimization for PU80.

# 4 Summary and Conclusion

In this study, we developed a fully-automated 2-step FEM simulation model to efficiently study the acoustic performance of underwater polyurethane acoustic coatings with 2 layers of embedded cylindrical voids, while accounting for the impact of hydrostatic pressure and frequency-dependent complex moduli. Our automated 2-step model removed the cumbersome manual transfer of information between steps. Furthermore, we integrated our 2-step FEM with a Bayesian optimization (BO) framework in a design loop, which allowed us to efficiently perform topology and layout optimization of voids throughout the matrix material for a 10-D design space. This framework enabled accelerated design of acoustic coatings with targeted performance, while overcoming the challenges brought by hydrostatic pressure to the

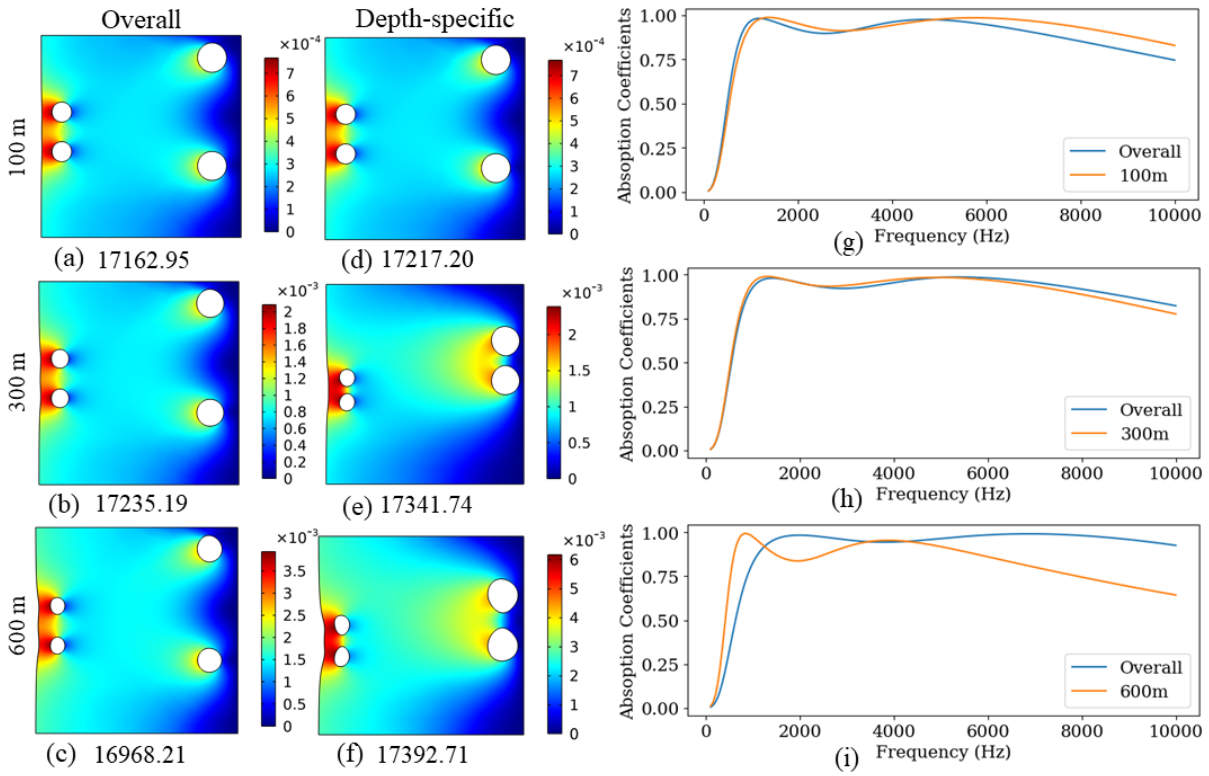


**Fig. 11**: **a-c** Deformation of the overall optimal design caused by the hydrostatic pressure, with their objective values at 100 m **(a)**, 300 m **(b)** and 600 m **(c)**, unit: **m**. **d-f** The depth-specific designs and their deformations caused by hydrostatic pressure at their designated depths: 100 m **(d)**, 300 m **(e)** and 600 m **(f)**, unit: **m**. The comparison of the absorption coefficient curves between overall optimal design and depth-specific design at each designated depth.

development of FEMs. The constraints and penalties included in the objective function of the BO framework enhanced the efficient exploration of the feasible solution space.

We find that the hydrostatic pressure plays a vital role in the design of acoustic coatings, by 1) shifting the absorption peaks to the higher frequencies, 2) affecting the feasible range of design parameter values. We also notice that while the stiffer material allows for larger voids, radii alone does not guarantee better performance, as the acoustic attenuation is attributed to the complex interaction between intrinsic (e.g. dissipation as heat due to the viscoelasticity of the base material) and structural losses (Fabry-Pérot resonance due to the voids in the metamaterial matrix).

The results demonstrate that this approach achieves an effective topological design, ensuring desired acoustic performance across the target depths while preventing metamaterial collapse/-failure due to the hydrostatic pressure.

BO was employed to efficient explore the design space, accelerating the development of acoustic coatings with targeted performance. This approach serves as a practical tool for making effective use of computationally expensive FEM simulations.

## 4.1 Future Remarks

In this study we assumed the viscoelasticity of the PU matrix is not affected by its long-term exposure to harsh operational conditions of deep seawater and possible changes in its microstructure. However, exposure to hydrostatic pressure over the life of the platform can potentially have impact on polymer's mechanical properties [36] and lead to possible degradation [37]. Thus, for

a broader study on practical candidate materials, this change may need to be taken in to consideration through life-cycle assessment of the coatings.

The significant role of frequency-dependent viscoelastic moduli of the polyurethane matrix on the acoustic performance of these coatings underpins the critical need for bridging the polyurethane chemistry (molecular scale) [38–40] and bulk morphologies (mesoscale) into the realm of macroscopic viscoelastic behavior. This requires development and integration of several simulation techniques such as molecular dynamics simulations of polyurethane chemistry and phase field modeling of its bulk morphologies to macroscopic constitutive equation-based FEM as a possible future work.

We used a simple polynomial approximation for the master curve reconstruction to represent the viscoelastic properties of the PU matrices, which is efficient given there are only 3 candidate materials. However in future study, when exploring broader range of materials, other physics-based constitutive models such as Prony series [41–43] and fractional viscoelastic [44–46] models could be adopted.

# Statements and Declarations

## Author Contributions

P. Ding: conceptualization, methodology, software, validation, analysis, investigation, writing - original draft, visualization. D. Robe: conceptualization, methodology, writing - reviewing and editing, supervision - supporting. M. Kirley, methodology, supervision - supporting, writing - reviewing and editing. E. Hajizadeh: ideation, conceptualization, methodology, supervision, writing - reviewing and editing.

## Replication of Results

The algorithm used to produce these results is fully described within this manuscript. All packages and models that supported this study are publicly available. Optimization runs were performed repeatedly with different random number generator seeds. We have reported means and uncertainty bounds on these results to ensure reproducibility. Design variable ranges are also specified. Source code may be obtained from the corresponding author upon reasonable request.

- Conflict of Interest - None to declare
- Funding - None to declare
- Ethics approval and consent to participate - Not applicable
- Data availability - Source code to generate data may be obtained from the corresponding author upon reasonable request.

# Acknowledgment

P. Ding is supported by the research training program (RTP) scholarship provided by the Australian government.

# References

[1] Zhu, Z., Hu, N., Wu, J., Li, W., Zhao, J., Wang, M., Zeng, F., Dai, H., Zheng, Y.: A review of underwater acoustic metamaterials for underwater acoustic equipment. Frontiers in Physics **10**, 1068833 (2022)

[2] Jayakumari, V., Shamsudeen, R., Rajeswari, R., Mukundan, T.: Viscoelastic and acoustic characterization of polyurethane-based acoustic absorber panels for underwater applications. Journal of Applied Polymer Science **136**(10), 47165 (2019)

[3] Liu, Z., Zhang, X., Mao, Y., Zhu, Y.Y., Yang, Z., Chan, C.T., Sheng, P.: Locally resonant sonic materials. science **289**(5485), 1734–1736 (2000)

[4] Sharma, G.S., Skvortsov, A., MacGillivray, I., Kessissoglou, N.: Sound absorption by rubber coatings with periodic voids and hard inclusions. Applied Acoustics **143**, 200–210 (2019) https://doi.org/10.1016/j.apacoust.2018.09.003

[5] Sharma, G.S., Skvortsov, A., MacGillivray, I., Kessissoglou, N.: Sound transmission through a periodically voided soft elastic medium submerged in water. Wave Motion **70**, 101–112 (2017) https://doi.org/10.1016/j.wavemoti.2016.10.006 . Recent Advances on Wave Motion in Fluids and Solids

[6] Sharma, G.S., Skvortsov, A., MacGillivray, I., Kessissoglou, N.: Acoustic performance of gratings of cylindrical voids in a soft elastic medium with a steel backing. The Journal of the Acoustical Society of America **141**(6), 4694–4704 (2017)

[7] Sharma, G.S., Faverjon, B., Dureisseix, D., Skvortsov, A., MacGillivray, I., Audoly, C., Kessissoglou, N.: Acoustic performance of a periodically voided viscoelastic medium with uncertainty in design parameters. Journal of Vibration and Acoustics **142**(6), 061002 (2020) https://doi.org/10.1115/1.4046859

[8] Gaunaurd, G., Callen, E., Barlow, J.: Pressure effects on the dynamic effective properties of perforated resonating elastomers. The Journal of the Acoustical Society of America **75**(S1), 16–16 (1984)

[9] Fu, Y., Wang, H., Cao, P.: Numerical design and optimization of metamaterials for underwater sound absorption at various hydrostatic pressures. Journal of Low Frequency Noise, Vibration and Active Control **42**(3), 1434–1450 (2023)

[10] Fang, X., Pan, X., Zhang, X., Li, D., Yin, X., Jin, Y., Wang, W., Wu, W.: Investigation on low-frequency and broadband sound absorption of the compact anechoic coating considering hydrostatic pressure. Journal of Marine Science and Engineering **12**(4) (2024) https://doi.org/10.3390/jmse12040543

[11] Hajizadeh, E., Todd, B.D., Daivis, P.J.: Nonequilibrium molecular dynamics simulation of dendrimers and hyperbranched polymer melts undergoing planar elongational flow. J. Rheol. **58**(2), 281–305 (2014)

[12] Hajizadeh, E., Todd, B.D., Daivis, P.J.: Shear rheology and structural properties of chemically identical dendrimer-linear polymer blends through molecular dynamics simulations. J. Chem. Phys. **141**(19), 194905 (2014)

[13] Hajizadeh, E., Todd, B.D., Daivis, P.J.: A molecular dynamics investigation of the planar elongational rheology of chemically identical dendrimer-linear polymer blends. J. Chem. Phys. **142**(17), 174911 (2015)

[14] Weeratunge, H., Shireen, Z., Iyer, S., Menzel, A., Phillips, A.W., Halgamuge, S., Sandberg, R., Hajizadeh, E.: A machine learning accelerated inverse design of underwater acoustic polyurethane coatings. Structural and Multidisciplinary Optimization **65**(8), 213 (2022) https://doi.org/10.1007/s00158-022-03322-w . Accessed 2024-04-15

[15] Panisilvam, J., Hajizadeh, E., Weeratunge, H., Bailey, J., Kim, S.: Asymmetric cyclegans for inverse design of photonic metastructures. APL Machine Learning **1**(4), 046105 (2023)

[16] Donti, P.L., Rolnick, D., Kolter, J.Z.: DC3: A learning method for optimization with hard constraints (2021) https://doi.org/10.48550/ARXIV.2104.12225 . Publisher: arXiv Version Number: 1. Accessed 2025-02-24

[17] Abdolahi, J., Robe, D., Larson, R., Kirley, M., Hajizadeh, E.: Interpretable active learning meta-modeling for the association dynamics of telechelic polymers on colloidal particles. Journal of Rheology **69**(2), 183–199 (2025)

[18] Gelbart, M.A., Snoek, J., Adams, R.P.: Bayesian Optimization with Unknown Constraints. arXiv. Version Number: 1 (2014). https://doi.org/10.48550/ARXIV.1403.5607 . https://arxiv.org/abs/1403.5607 Accessed 2025-02-24

[19] Gardner, J., Kusner, M., Zhixiang, Weinberger, K., Cunningham, J.: Bayesian optimization with inequality constraints. In: Xing, E.P., Jebara, T. (eds.) Proceedings of the 31st International Conference on Machine Learning. Proceedings of Machine Learning Research, vol. 32, pp. 937–945. PMLR, Bejing, China (2014)

[20] Weeratunge, H., Robe, D., Menzel, A., Phillips, A.W., Kirley, M., Smith-Miles, K., Hajizadeh, E.: Bayesian coarsening: rapid tuning of polymer model parameters. Rheologica Acta **62**(10), 477–490 (2023)

[21] Robe, D., Menzel, A., Phillips, A., Hajizadeh, E.: Smiles to scattering: Automated high-throughput atomistic polyurethane simulations compared with waxs data. Computatioanl Materials Science **256**, 113931 (2025) https://doi.org/10.1016/j.commatsci.2025.113931

[22] Zou, M.-S., Liu, S.-X., Jiang, L.-W., Huang, H.: A mixed analytical-numerical method for the acoustic radiation of a spherical double shell in the ocean-acoustic environment. Ocean Engineering **199**, 107040 (2020) https://doi.org/10.1016/j.oceaneng.2020.107040

[23] Hennig, J., Elfner, M., Maeder, A., Feder, J.: MPh-py/MPh: 1.2.4. https://doi.org/10.5281/zenodo.11539226 . https://doi.org/10.5281/zenodo.11539226

[24] Nelson, K.E., Scherer, M.K., Administration, U.N.N.S.: JPype (2020). https://doi.org/10.11578/dc.20201021.3 . https://www.osti.gov/biblio/1679973

[25] Sharma, G.S., Skvortsov, A., MacGillivray, I., Kessissoglou, N.: Acoustic performance of gratings of cylindrical voids in a soft elastic medium with a steel backing **141**(6), 4694–4704 https://doi.org/10.1121/1.4986941 . Accessed 2025-03-27

[26] Jayakumari, V.G., Shamsudeen, R.K., Ramesh, R., Mukundan, T.: Modeling and validation of polyurethane based passive underwater acoustic absorber **130**(2), 724–730 https://doi.org/10.1121/1.3605670 . Accessed 2025-03-27

[27] Jones, D.R., Schonlau, M., Welch, W.J.: Efficient global optimization of expensive black-box functions. Journal of Global optimization **13**, 455–492 (1998)

[28] Shahriari, B., Swersky, K., Wang, Z., Adams, R.P., Freitas, N.: Taking the human out of the loop: A review of bayesian optimization. Proceedings of the IEEE **104**(1), 148–175 (2016) https://doi.org/10.1109/JPROC.2015.2494218

[29] Hajizadeh, E., Garmabi, H.: Response surface based optimization of toughness of hybrid polyamide 6 nanocomposites. International Journal of Chemical & Biomolecular Engineering **1**(1), 40–44 (2008)

[30] Xu, Z., Wang, H., Phillips, J.M., Zhe, S.: Standard Gaussian Process Can Be Excellent for High-Dimensional Bayesian Optimization. arXiv. arXiv:2402.02746 [cs] (2024). https://doi.org/10.48550/arXiv.2402.02746 . http://arxiv.org/abs/2402.02746 Accessed 2025-02-24

[31] Bian, C., Wang, X., Liu, C., Xie, X., Haitao, L.: Impact of exploration-exploitation trade-off on UCB-based Bayesian Optimization. IOP Conference Series: Materials Science and Engineering **1081**(1), 012023 (2021) https://doi.org/10.1088/1757-899X/1081/1/012023 . Accessed 2025-02-24

[32] Nogueira, F.: Bayesian Optimization: Open source constrained global optimization tool for Python (2014–). https://github.com/bayesian-optimization/BayesianOptimization

[33] Gaunaurd, G., Callen, E., Barlow, J.: Effect of pressure on the static and dynamic acoustic properties of porous rubber (1983)

[34] Thieury, M., Tourin, A., Dasse, J., Leroy, V.: Effect of hydrostatic pressure on a bubble anechoic metascreen. In: 13th Internaional Congress on Artificial Materials for Novel Wave Phenomena-Metamaterials (2019)

[35] Levin, C., Sharma, G.S., MacGillivray, I., Skvortsov, A., Kessissoglou, N.: Acoustic performance of a voided soft medium under hydrostatic pressure. Proc Acoust **21**(23), 2022 (2021)

[36] Hoppel, C.P.R., Bogetti, T.A., John W. Gillespie, J.: Effects of hydrostatic pressure on the mechanical behavior of composite materials. Technical Report ARL-TR-727, U.S. Army Research Laboratory, Aberdeen Proving Ground, MD (April 1995). Approved for public release; distribution is unlimited.

[37] Beretti, S., Audoly, C., Guillaussier, P.: Pressure effects on the dynamic and static properties of perforated elastomers used in underwater acoustics. The Journal of the Acoustical Society of America **97**(5_Supplement), 3293–3293 (1995)

[38] Shireen, Z., Weeratunge, H., Menzel, A., Phillips, A.W., Larson, R.G., Smith-Miles, K., Hajizadeh, E.: A machine learning enabled hybrid optimization framework for efficient coarse-graining of a model polymer. npj Computational Materials **8**(1), 224 (2022)

[39] Robe, D., Menzel, A., Phillips, A.W., Hajizadeh, E.: Procedural construction of atomistic polyurethane block copolymer models for high throughput simulations. arXiv preprint arXiv:2405.15226 (2024)

[40] Shireen, Z., Hajizadeh, E., Daivis, P., Brandl, C.: Molecular dynamics study of the linear viscoelastic shear and bulk relaxation moduli of poly(tetramethylene oxide) (PTMO) (2022) https://doi.org/10.48550/ARXIV.2202.08993 . Publisher: [object Object] Version Number: 1. Accessed 2024-04-15

[41] Ghoreishy, M.H.R.: Determination of the parameters of the Prony series in hyper-viscoelastic material models using the finite element method. Materials & Design **35**, 791–797 (2012) https://doi.org/10.1016/j.matdes.2011.05.057 . Accessed 2025-02-24

[42] Park, S.W., Schapery, R.A.: Methods of interconversion between linear viscoelastic material functions. Part I—a numerical method based on Prony series. International Journal of Solids and Structures **36**(11), 1653–1675 (1999) https://doi.org/10.1016/S0020-7683(98)00055-9 . Accessed 2025-02-24

[43] Chen, T.: Determining a prony series for a viscoelastic material from time strain data. US Army Res. Lab.: Fort Belvoir, VA, USA (2000)

[44] Xiao, R., Sun, H., Chen, W.: An equivalence between generalized Maxwell model and fractional Zener model. Mechanics of Materials **100**, 148–153 (2016) https://doi.org/10.1016/j.mechmat.2016.06.016

[45] Bonfanti, A., Kaplan, J.L., Charras, G., Kabla, A.: Fractional viscoelastic models for power-law materials. Soft Matter **16**(26), 6002–6020 (2020) https://doi.org/10.1039/D0SM00354A . Accessed 2025-02-24

[46] Shen, L.-J.: Fractional derivative models for viscoelastic materials at finite deformations. International Journal of Solids and Structures **190**, 226–237 (2020) https://doi.org/10.1016/j.ijsolstr.2019.10.025 . Accessed 2025-02-24